# IETA International Information and Engineering Technology Association

#### **Mathematical Modelling of Engineering Problems**

Vol. 12, No. 10, October, 2025, pp. 3335-3347

Journal homepage: http://iieta.org/journals/mmep

## Hierarchical Multizeolitic Purification System for Upgrading Waste Frying Oil into High-Quality Biodiesel Feedstock



Sudipta Dasgupta<sup>1</sup>, Mohuli Das<sup>2</sup>, Marcos Antônio Klunk<sup>3</sup>, Soyane Juceli Siqueira Xavier<sup>4</sup>, Ayush Srivastava<sup>1</sup>, Giulio Lorenzini<sup>5\*</sup>, Nattan Roberto Caetano<sup>6</sup>

- <sup>1</sup> Department of Earth Sciences, Indian Institute of Technology Bombay (IIT Bombay), Mumbai 400076, India
- <sup>2</sup> Department of Petroleum Engineering and Earth Sciences, Indian Institute of Petroleum and Energy (IIPE), Visakhapatnam 530003, India
- <sup>3</sup> Geology and Geophysics Research Group NGA, University of Vale do Rio dos Sinos, São Leopoldo 93022750, Brazil
- <sup>4</sup> Department of Geology, University of Vale do Rio dos Sinos, São Leopoldo 93022750, Brazil
- <sup>5</sup> Department of Industrial Systems and Technologies Engineering, University of Parma, Parma 43124, Italy
- <sup>6</sup> Department of Mechanical Engineering, Federal University of Santa Maria, Santa Maria 97105900, Brazil

Corresponding Author Email: giulio.lorenzini@unipr.it

Copyright: ©2025 The authors. This article is published by IIETA and is licensed under the CC BY 4.0 license (http://creativecommons.org/licenses/by/4.0/).

https://doi.org/10.18280/mmep.121001

#### Received: 16 July 2025 Revised: 4 September 2025 Accepted: 11 September 2025 Available online: 31 October 2025

#### Keywords:

zeolites, biodiesel, valorization of waste oils, aluminosilicate, cation exchange capacity, free fatty acids, rice husk ash

#### **ABSTRACT**

The development of sustainable biodiesel production depends on cost-effective and renewable feedstocks that minimize environmental impact without compromising fuel quality. Waste frying oil (WFO) is a promising alternative due to its abundance, yet its high content of water, free fatty acids (FFAs), and polymerized oxidation products severely hinders transesterification efficiency. This study introduces a hierarchical multizeolitic purification system engineered to sequentially eliminate these contaminants through targeted adsorption. Four zeolites with complementary pore architectures and acidities-4A (LTA), Beta (BEA), Y (FAU), and ZSM-5 (MFI)were hydrothermally synthesized from rice husk ash and metakaolin and assembled in a serial adsorption column. Each zeolite was assigned a specific role: dehydration (4A), removal of polymerized and oxidized species (Beta), adsorption of long-chain FFAs (Y), and final polishing of aromatic and oxygenated residues (ZSM-5). The integrated process markedly enhanced WFO quality, reducing moisture from 1166 mg·kg<sup>-1</sup> to 200 mg·kg<sup>-1</sup>, acid value from 2.65 to 0.59 mg KOH·g<sup>-1</sup>, peroxide value from 14.16 to 4.9 meq O<sub>2</sub>·kg<sup>-1</sup>, and viscosity from 43.1 to 37.1 mm<sup>2</sup>·s<sup>-1</sup>, while improving oxidative stability from 4.8 h to 6.7 h. Fatty acid profiling confirmed a reduction in polyunsaturated species and enrichment in thermally stable monounsaturated and saturated fractions. The proposed system demonstrates an efficient, scalable, and environmentally benign approach for converting waste oils into high-quality biodiesel feedstock, aligning with green chemistry and circular economy principles.

#### 1. INTRODUCTION

The rising global demand for fuels, combined with growing concerns about the environmental impacts of fossil fuel combustion, has driven the search for renewable and sustainable alternatives [1, 2]. In this context, biodiesel emerges as a promising option to partially or fully replace mineral diesel, offering advantages such as lower atmospheric pollutant emissions, high biodegradability, and reduced toxicity [3-6]. Biodiesel is traditionally obtained through the transesterification or esterification of vegetable oils and animal fats with short-chain alcohols, such as methanol, in the presence of homogeneous or heterogeneous catalysts, resulting in the formation of methyl esters and glycerol [7-10]. Despite its environmental benefits, large-scale biodiesel production still faces economic challenges, mainly due to the high cost of refined vegetable oils, which can account for up to 80% of the total process investment [11-14].

As a cost-reduction strategy aligned with the principles of the circular economy, the use of WFO has gained significant attention [15, 16]. Beyond its lower price, this feedstock contributes to the recovery of residues generated in large volumes, mitigating the impacts associated with improper disposal into the environment [17, 18]. However, the quality of these oils is compromised by successive heating cycles that lead to the formation of free fatty acids, peroxides, polymers, moisture, and solid contaminants, making the transesterification process more difficult and reducing the quality of the final biodiesel [19].

During frying, oil is exposed to temperatures between 160 and 220°C for prolonged periods, in contact with air. These conditions promote oxidation and polymerization reactions, leading to increased acidity, viscosity, and oxidative instability [20, 21]. The presence of free fatty acids above 1% and water can trigger saponification in alkaline systems, reducing the reaction yield and forming emulsions that hinder

product separation. While homogeneous acid catalysis can be a technical alternative, it also presents limitations, such as equipment corrosion and the generation of acidic effluents [22]. Therefore, the preliminary purification of WFO becomes a crucial step to enable its use as a feedstock in biodiesel production [23]. Among pretreatment technologies, the use of zeolites as selective and multifunctional adsorbent materials stands out [24, 25]. These properties confer a high affinity for both polar and nonpolar compounds present in waste oils, enabling the controlled removal of water, free fatty acids, polymers, and oxidation products [26, 27].

Zeolites are crystalline aluminosilicate minerals with a porous structure, formed by a three-dimensional network of silica (SiO<sub>4</sub>) and alumina (AlO<sub>4</sub>) tetrahedra, interconnected by oxygen atoms [28-31]. This structure contains uniform channels and cavities, typically ranging from 3 to 10 Å, making them microporous materials [32]. They exhibit properties such as high cation exchange capacity (CEC), molecular selectivity, and adsorption ability, and are widely used in applications like desalination, catalysis (e.g., cracking in oil refining), and gas separation [33-35].

Zeolite 4A is a synthetic aluminosilicate with a crystalline structure, classified under the LTA (Linde Type A) zeolite family. Its idealized formula, Na<sub>12</sub>[(AlO<sub>2</sub>)<sub>12</sub>(SiO<sub>2</sub>)<sub>12</sub>]·27H<sub>2</sub>O, reflects a Si/Al molar ratio near 1 [36]. This low ratio enhances its hydrophilicity and provides a high CEC, typically 4-5 meq·g<sup>-1</sup> [37]. Structurally, it features a cubic arrangement of α-cages linked by eight-membered ring windows, approximately 0.41 nm wide. This allows selective adsorption of small molecules (e.g., H2O, NH3, CO2) with kinetic diameters under 4 Å [38]. This property is widely used in industrial applications like gas and liquid dehydration, organic stream purification, and moisture control in oils and fuels [39]. In WFO purification, zeolite 4A excels at removing free and bound water, residual alcohols, and small polar molecules. This prevents hydrolysis and saponification, which could reduce transesterification efficiency [40]. Texturally, it offers high microporosity with a micropore volume of 0.20-0.25 cm<sup>3</sup>·g<sup>-1</sup> and a BET surface area of 350-400 m<sup>2</sup>·g<sup>-1</sup>, with minimal mesoporosity [41]. It remains thermally stable up to 800°C but is less resistant to prolonged exposure to strong acids or bases due to potential aluminum leaching and framework breakdown [42]. In multizeolite systems, zeolite 4A initiates purification by reducing moisture and polar contaminants, setting the stage for further processing [43].

Beta zeolite is a high-silica aluminosilicate with a three-dimensional framework, classified as BEA-type by the International Zeolite Association [44]. Its formula, (Na<sup>+</sup>, H<sup>+</sup>)[(AlO<sub>2</sub>)<sub>x</sub>(SiO<sub>2</sub>)<sub>y</sub>]·zH<sub>2</sub>O, features a variable Si/Al ratio (5–150), adjustable based on synthesis conditions and intended use [45]. This flexibility allows tuning of acidity, hydrophobicity, and thermal stability. Its structure includes 12-membered ring channels (0.66–0.76 nm), enabling adsorption of larger molecules like aromatics and polymeric oxidation products [46].

This makes it valuable for purifying WFO, which often contains polymers from extended heating [47]. Texturally, it offers a BET surface area of 500–700 m²·g⁻¹, a micropore volume of 0.20–0.25 cm³·g⁻¹, and secondary mesoporosity (0.10–0.15 cm³·g⁻¹) from defects or treatments [48-50]. Its Brønsted acidity, from Si⁴+ to Al³+ substitution, can be adjusted via the Si/Al ratio to optimize contaminant interactions [51]. In multizeolite systems, Beta follows 4A, targeting larger, less polar compounds to complement the

initial dehydration step [52].

It remains stable above 800°C and resists neutral to mildly acidic conditions [53]. This combination of properties positions Beta as an effective second stage in WFO purification, reducing high-molecular-weight contaminants and enhancing oil quality for transesterification [54]. Zeolite Y, part of the FAU (faujasite) group, is a crystalline aluminosilicate with a three-dimensional framework of supercages connected by 12-membered ring windows, offering a pore diameter of about 0.74 nm [55, 56]. Its formula,  $M_x/n[(AlO_2)_x(SiO_2)_\gamma].zH_2O$ , includes charge-compensating cations (e.g.,  $Na^+$ ,  $H^+$ ) and variable water content [57, 58].

It boasts a BET surface area of 700–900 m<sup>2</sup>·g<sup>-1</sup> and a micropore volume of 0.30–0.40 cm<sup>3</sup>·g<sup>-1</sup>, ideal for adsorbing bulky molecules like FFAs and oxidized compounds in WFO [59]. Its acidity, featuring both Brønsted and Lewis sites, varies with the Si/Al ratio (2–5 for hydrophilicity, higher for hydrophobicity), enhancing interactions with polar or nonpolar contaminants [60]. In multizeolite systems, zeolite Y follows Beta, targeting long-chain FFAs, peroxides, and midsized contaminants to improve oil acidity and oxidative stability before transesterification [61, 62].

It withstands temperatures up to 800°C and remains durable in moderately alkaline conditions [63]. Its large pores, high micropore volume, and tunable acidity make it an essential intermediate stage in WFO purification, preparing the oil for the final polishing with ZSM-5 [64]. ZSM-5, an MFI-type aluminosilicate, features a three-dimensional network of intersecting channels with 10-membered rings, offering a pore diameter of about 0.55 nm. Its formula,  $M_x/n[(AlO_2)_x(SiO_2)_y]\cdot zH_2O$ , includes cations like Na<sup>+</sup> or H<sup>+</sup> [65, 66]. With a Si/Al ratio of 25 to over 1000, ZSM-5 is highly hydrophobic, excelling at adsorbing nonpolar or weakly polar molecules.

In WFO purification, it targets aromatics, residual peroxides, and low-molecular-weight FFAs remaining after earlier stages [67, 68]. Its BET surface area ranges from 350–450 m<sup>2</sup>·g<sup>-1</sup>, with a micropore volume of 0.10–0.15 cm<sup>3</sup>·g<sup>-1</sup> and occasional mesoporosity, ensuring effective "polishing" despite a lower total pore volume [69, 70]. ZSM-5's acidity, with moderate Brønsted and Lewis sites, is adjustable via the Si/Al ratio, aiding retention of oxygenated and polar residues without structural damage [71-73].

As the final stage in multizeolite WFO systems, it removes small aromatic and oxidized species after 4A (water), Beta (polymers), and Y (FFAs), ensuring low acidity and high oxidative stability for transesterification [74, 75]. In multizeolite WFO purification systems, ZSM-5 is positioned as the final stage. Following the initial removal of water (4A), polymers (Beta), and long-chain FFAs (Y), ZSM-5 adsorbs smaller, aromatic, and persistent oxidized species, ensuring that the purified oil has low acidity, high oxidative stability, and a composition suitable for transesterification. ZSM-5's thermal stability (up to 800°C) and chemical resistance ensure consistent performance over multiple cycles, making it the ideal final polisher for WFO, enhancing feedstock quality for biodiesel production [76, 77].

Combining different types of zeolites in sequential purification systems is an innovative approach that allows the complementary use of their textural and chemical properties [78].

In this study, a purification system composed of multiple zeolites arranged in series is proposed, with each type playing a specific role in contaminant removal. Zeolite 4A is employed in the initial stage for the removal of polar molecules, particularly water and residual alcohols. Next, Beta zeolite (BEA) is used to adsorb larger molecules, such as polymers formed during prolonged oil use.

Finally, zeolites Y and ZSM-5 are applied complementarily to selectively capture free fatty acids and smaller compounds, ensuring a high degree of purification before the transesterification stage. This strategy aims not only to improve the physicochemical properties of waste frying oil but also to reduce production costs and enhance residue valorization, thereby contributing to the advancement of clean, economically viable technologies for sustainable biodiesel production.

#### 2. MATERIALS AND METHODS

#### 2.1 Raw materials

The used frying oil was obtained from a vegetable oil recycling center located in the metropolitan region of Porto Alegre, RS, and comes from the waste of restaurants and large establishments that work with fried foods. The rice husk ash (RHA) was obtained from a thermoelectric power plant in Rio Grande do Sul, Brazil, which uses biomass for energy generation, while the metakaolin (MK) was produced by the calcination of kaolinite ( $Al_2Si_2O_5(OH)_4$ ) [79-81]. The compositions of the eco-friendly materials were determined by X-ray fluorescence (XRF), as presented in Table 1.

**Table 1.** Chemical analysis of the compounds present in the rice husk ash and metakaolin (% mass)

Oxides	RHA	MK
SiO <sub>2</sub>	99.12	52.58
$Al_2O_3$	0.10	38.44
$Fe_2O_3$	0.03	2.11
Na <sub>2</sub> O	-	0.04
$K_2O$	0.64	0.55
CaO	-	2.06
MgO	-	0.97
$TiO_2$	-	2.47
$SO_3$	0.04	-
SiO <sub>2</sub> /Al <sub>2</sub> O <sub>3</sub>	981.38	1.36

#### 2.2 Zeolite synthesis

The synthesis of zeolites 4A, BEA, zeólitas Y e ZSM-5 was performed according to Kirdeciler and Akata [82], Chaikittisilp et al. [83], Dasgupta et al. [84] and Klunk et al. [81] respectively which has been optimized in this particular research work. The zeolites were acquired through hydrothermal synthesis in the hydrodynamic reactor (storage volume is 500 mL).

Tetramethylammonium hydroxide (TMAOH, 40% by weight) was employed as the organic structure-directing agent (OSDA) for the synthesis of zeolite 4A and zeolite Y [85, 86]. Tetraethylammonium hydroxide (TEAOH, 40% by weight) was used as the OSDA for Beta zeolite, while tetrapropylammonium hydroxide (TPAOH, 40% by weight) was selected for ZSM-5 [87, 88]. Sodium hydroxide (NaOH, 98%) was applied as the alkalizing agent. To obtain zeolite 4A (Si/Al = 1), Beta zeolite (Si/Al = 5), zeolite Y (Si/Al = 3.5), and ZSM-5 (Si/Al = 50), the relative proportions of rice husk ash and metakaolin were calculated based on their respective

SiO<sub>2</sub> and Al<sub>2</sub>O<sub>3</sub> contents.

The synthesis gels were prepared with a final volume of 500 mL, maintaining a total solids concentration of 10% (w/v). The specific quantities of each component used in the formulations are presented in Table 2.

**Table 2.** Reagent quantities used in the synthesis of zeolitic material

Zeolite	RHAa	MKa	OSDA <sup>a</sup>	NaOHa	H <sub>2</sub> O <sup>b</sup>
4A	5.08	13.15	TMAOH – 2.33	3.36	476.11
BEA	25.87	8.11	TEAOH – 6.11	2.77	457.92
Y	15.22	9.83	TMAOH - 4.53	3.12	468.28
ZSM-5	45.97	4.53	TPAOH - 20.83	1.65	429.07

Note: a grams; b mL

#### 2.3 Material characterization

The synthesized zeolites were characterized using a comprehensive set of analytical techniques. The specific surface area was determined by the Brunauer–Emmett–Teller (BET) method, while textural properties were evaluated through N<sub>2</sub> adsorption/desorption isotherms at 77 K. Total acidity was quantified by temperature-programmed desorption of ammonia (NH<sub>3</sub>-TPD), and functional groups were identified using Fourier-Transform Infrared (FTIR). Thermal stability was assessed by thermogravimetric analysis (TGA). The physicochemical properties and FTIR spectra of the waste frying oil (WFO) were analyzed before and after purification to evaluate the contaminant removal efficiency of the zeolitic materials.

### 2.4 Purification of waste frying oil through molecular sieves

For the purification stage of the WFO, a multi-bed adsorption system was designed with beds arranged in series, each containing a zeolite with specific properties, in order to promote the selective and progressive removal of the main contaminants present in the feedstock (Figure 1).

This modular arrangement allows each adsorption unit to operate independently, enhancing overall efficiency while simplifying maintenance and replacement of adsorbent materials. In the first stage, a bed of zeolite 4A was employed, characterized by an effective pore diameter of approximately 0.4 nm and a high affinity for low molecular weight polar molecules. This unit was positioned at the inlet due to its ability to remove both free and bound water, as well as residual alcohols present in the oil. Preliminary water removal is essential to prevent triglyceride hydrolysis and free fatty acid formation, which can impair the efficiency of the subsequent transesterification step.

Next, the partially dehydrated oil stream was directed to a bed containing Beta zeolite. This zeolite features a three-dimensional channel system of approximately 0.66 nm in diameter and was employed to adsorb larger molecules and degradation products, such as polymers and oxidized compounds formed during prolonged frying. The removal of these contaminants contributes to viscosity reduction and improvement of the visual quality of the oil. In the third stage, the oil passes through a bed packed with zeolite Y. This zeolite exhibits large cavities, with an average diameter of around 0.74 nm, and a high capacity for retaining long-chain free fatty acids and medium molecular weight organic compounds. This step targets acidity reduction and minimizes soap formation

during alkaline transesterification.

Finally, the purified oil is directed to the bed containing ZSM-5 zeolite. This zeolite possesses one-dimensional channels of approximately 0.55 nm and exhibits high hydrophobicity, functioning as the final polishing stage. ZSM-5 removes residual free fatty acids and smaller compounds that may not have been retained in the preceding stages. The seriesconnected system was equipped with peristaltic pumps for controlled oil flow and vacuum pumps connected to each

module, enabling operation under reduced pressure and facilitating passage through the beds. Each adsorption unit was separated by cotton and glass wool plugs to contain particulate material and ensure uniform fluid distribution across the bed. This serial configuration allows for the synergistic utilization of the distinct adsorption capabilities of the zeolites, resulting in oil with significantly reduced contaminant levels, suitable for use in transesterification processes aimed at biodiesel production.

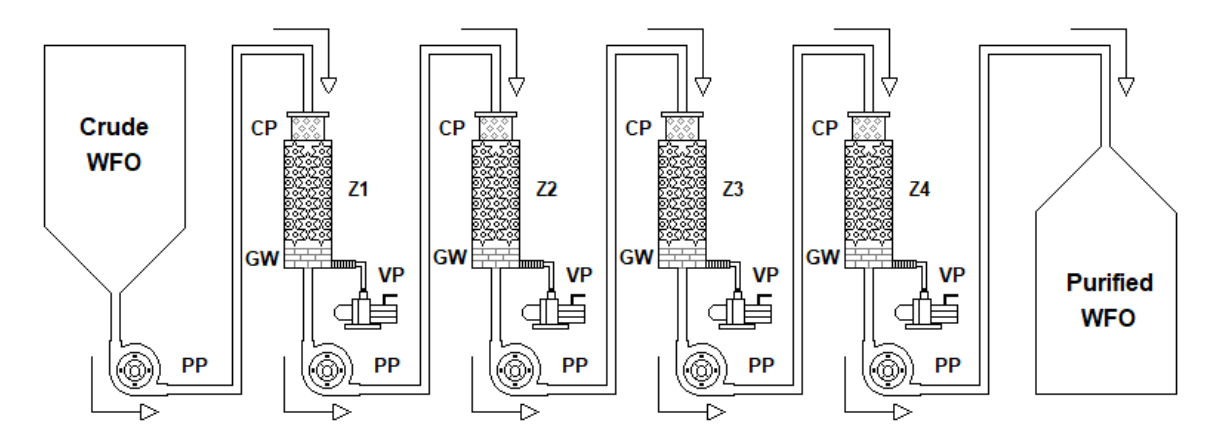


**Figure 1.** Schematic representation of the sequential adsorption system for waste frying oil purification using zeolite Note: Z1 – zeolite 4A; Z2 – Beta zeolite; Z3 – zeolite Y; Z4 – zeolite ZSM-5; PP – peristaltic pump; CP – cotton plug; GW – glass wools; VP – vacuum pump

#### 3. RESULTS AND DISCUSSION

#### 3.1 Characterization of zeolitic material

Table 3 presents the textural properties of the zeolitic materials employed, highlighting significant differences in surface area, micropore and mesopore volumes, and average pore diameter. These parameters are critical for understanding the selective adsorption potential of each zeolite in the removal of contaminants present in WFO.

**Table 3.** Reagent quantities used in the synthesis of zeolitic material

Zeolite	BET <sup>a</sup>	Micropore <sup>b</sup>	Mesoporec	APD <sup>d</sup>
4A	309	0.201	0.073	0.402
BEA	559	0.229	0.119	0.619
Y	701	0.354	0.101	0.332
ZSM-5	412	0.101	0.311	0.351

Note: a: surface area (m²/g); b: t-plot method; c: BJH method; APD: Average pore diameter (nm)

The results show that zeolite Y, with a Si/Al ratio of 5, exhibited the highest specific surface area (701 m²·g¹¹), followed by Beta (559 m²·g¹¹), ZSM-5 (412 m²·g¹¹), and 4A (309 m²·g¹¹). The high BET surface area of zeolite Y provides a large number of active sites for interaction with smaller molecules such as free fatty acids and secondary oxidation products. In contrast, the moderate surface area of zeolite 4A is adequate for the removal of water and small polar molecules but more limited in capturing higher molecular weight species. In terms of microporosity, zeolite Y also stood out, with a micropore volume of 0.354 cm³·g¹¹ significantly higher than Beta (0.229 cm³·g¹¹) and 4A (0.201 cm³·g¹¹). ZSM-5 displayed the lowest micropore volume (0.101 cm³·g¹¹), indicating a smaller contribution of intracrystalline micropores to adsorption. This profile suggests that zeolite Y plays a pivotal

role in the removal of smaller molecular species, while Beta primarily captures larger, partially polymerized fractions.

Mesoporosity showed an inverse trend relative to microporosity. ZSM-5 presented the highest mesopore volume (0.311 cm<sup>3</sup>·g<sup>-1</sup>), consistent with its unidimensional channel system that facilitates adsorption of bulkier species such as oligomers and resinous degradation products formed during prolonged frying.

Beta exhibited moderate mesoporosity (0.119 cm³·g¹¹), whereas zeolite Y was predominantly microporous (0.101 cm³·g¹¹). Zeolite 4A had the lowest mesopore volume (0.073 cm³·g¹¹), confirming its highly microporous nature and selectivity for small polar molecules such as water. Average pore diameter values further highlight key differences. Beta showed the largest average pore diameter (0.619 nm), consistent with its ability to capture larger contaminants.

Zeolite Y exhibited the smallest average pore diameter (0.332 nm), reflecting its high selectivity for small molecules. Zeolite 4A displayed an intermediate value (0.402 nm), ideal for moisture removal and trapping small impurities, while ZSM-5 had an average pore diameter of 0.351 nm, consistent with its role in final adsorption of aromatic and residual polar species.

Overall, the combined textural characteristics of the four zeolites justify their sequential application in the WFO purification system. Zeolite 4A, with low mesoporosity and high affinity for polar molecules, serves as the initial dehydration stage and removes residual alcohols. Beta, with larger pore diameter and high surface area, retains polymers and high-molecular-weight oxidation products.

Zeolite Y, with maximum microporosity and surface area, is critical for removing free fatty acids and low-molecular-weight contaminants. Finally, ZSM-5, with higher mesoporosity and unidimensional channels, acts as a final polishing stage, adsorbing aromatic fractions and minor residual compounds.

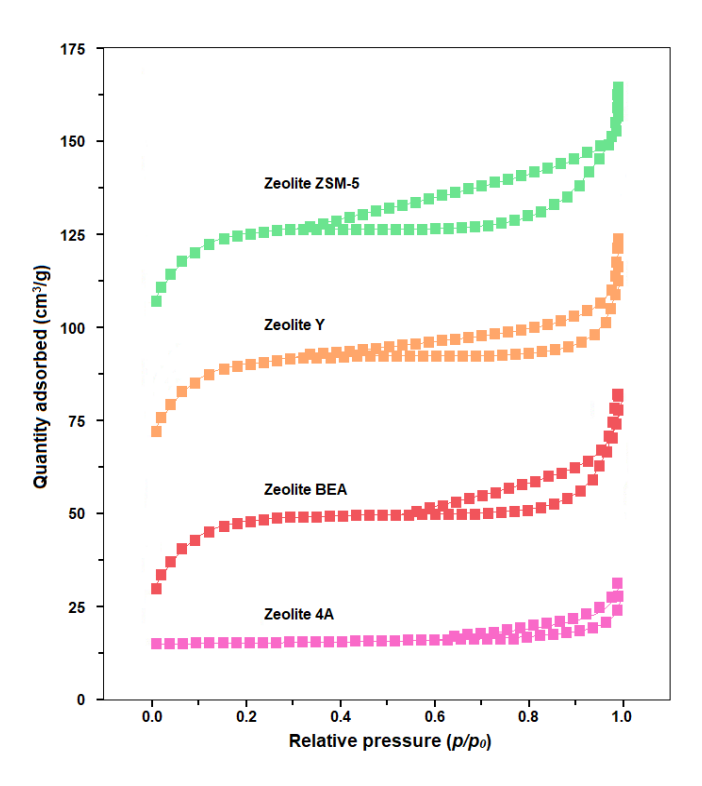


**Figure 2.** N<sub>2</sub> adsorption and desorption isotherm of the zeolitic materials

Figure 2 presents the  $N_2$  adsorption—desorption isotherms of the zeolitic materials employed in WFO purification. Analysis of these isotherms provides key insights into pore structure, surface area, and pore accessibility of each zeolite, parameters directly linked to their adsorption efficiency for contaminants in the oil. Zeolite 4A exhibits a Type I isotherm, characteristic of microporous materials, with low adsorption at higher relative pressures ( $p/p_0 > 0.8$ ) and a relatively modest total adsorption volume.

These data indicate the predominance of micropores with an effective diameter of approximately 0.4 nm and a moderate specific surface area. Despite its lower total adsorption capacity, 4A stands out for its high affinity toward low-molecular-weight polar molecules, such as water. This makes it particularly effective in the initial stage of the purification system, where moisture removal from WFO is essential to avoid undesirable reactions such as triglyceride hydrolysis.

Zeolite Beta (BEA) displays an isotherm with slight hysteresis at intermediate pressures, indicating the presence of mesopores in addition to its intrinsic micropores. This behavior is associated with its three-dimensional channel system with diameters of approximately 0.6 nm, which enables efficient adsorption of larger molecules, including polymers and oxidation products formed during prolonged oil heating. This property justifies its application immediately after 4A in the multizeolite system, targeting the removal of higher molecular weight species.

Zeolite Y exhibits the highest adsorption capacity among the microporous materials studied, with a pronounced Type I isotherm and a significantly greater total micropore volume. With pore diameters averaging around 0.74 nm and a specific surface area exceeding 700 m<sup>2</sup>·g<sup>-1</sup>, zeolite Y is highly efficient at capturing smaller oxidized compounds and free fatty acids present in WFO. These results underscore its critical role in the intermediate stage of purification, where the removal of oil-soluble contaminants is prioritized.

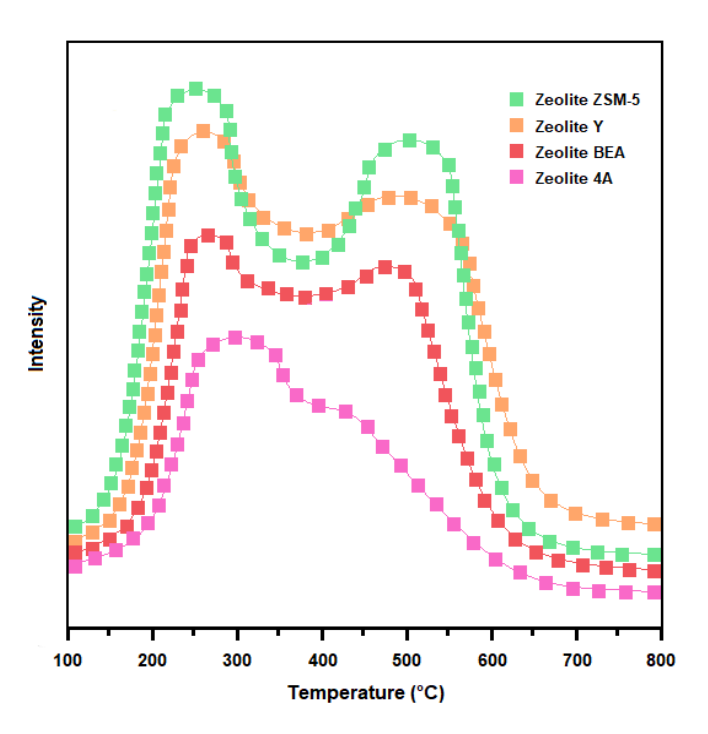


Figure 3. NH<sub>3</sub>-TPD profiles the zeolitic materials

Finally, zeolite ZSM-5 presents an intermediate isotherm profile, combining microporous features with moderate hysteresis. Its unidimensional channel system, with diameters of approximately 0.55 nm, favors the selective adsorption of molecules with specific geometry and moderate apolarity. This selectivity makes ZSM-5 well suited for the final stage of the process, acting as a "polishing" step by removing residual molecular species that were not captured in previous stages.

Figure 3 presents the temperature-programmed desorption of ammonia (NH<sub>3</sub>-TPD) profiles of zeolites 4A, BEA, Y, and ZSM-5, which provide crucial information on the quantity and strength of acid sites present in each material. The acidity of a zeolite directly influences its ability to chemically interact with species in the waste frying oil, such as free fatty acids and oxidized products, making this parameter fundamental in the WFO purification stage.

All samples exhibit two main desorption peaks: one in the range of 150-300°C, associated with weak acid sites, and another between 400-600°C, corresponding to moderate-tostrong acid sites. Zeolite ZSM-5 displayed the highest overall desorption signal, indicating the greatest total concentration of acid sites among the materials analyzed. Its second peak, particularly intense and shifted toward higher temperatures, evidences the presence of strong acid sites, consistent with its MFI-type framework, which is highly effective for adsorbing oxidized compounds and free fatty acids. Zeolite Y also showed high acidity, with two well-defined peaks, reflecting its capacity to interact with contaminants through both weak and strong acid sites. Its FAU-type structure, with large pore openings (~0.74 nm), facilitates the diffusion of larger molecules, enhancing its efficiency in the intermediate purification stage.

Zeolite BEA exhibited intermediate behavior in terms of both peak intensity and desorption temperature, confirming the presence of moderate-strength acid sites compatible with its role in retaining polymers and oxidation products formed during prolonged oil use. In contrast, zeolite 4A presented the lowest acidity profile, with less intense peaks concentrated at lower temperatures. This reinforces its application in the initial

stage of the process, primarily targeting the removal of water and small polar molecules rather than more complex organic contaminants.

Figure 4 presents the FTIR spectra of ZSM-5, Y, BEA, and 4A zeolites. The characteristic bands observed in the spectra confirm the presence of functional groups and framework vibrations typical of their respective crystalline networks, providing important insights into the identity and structural integrity of the materials employed in the purification of WFO.

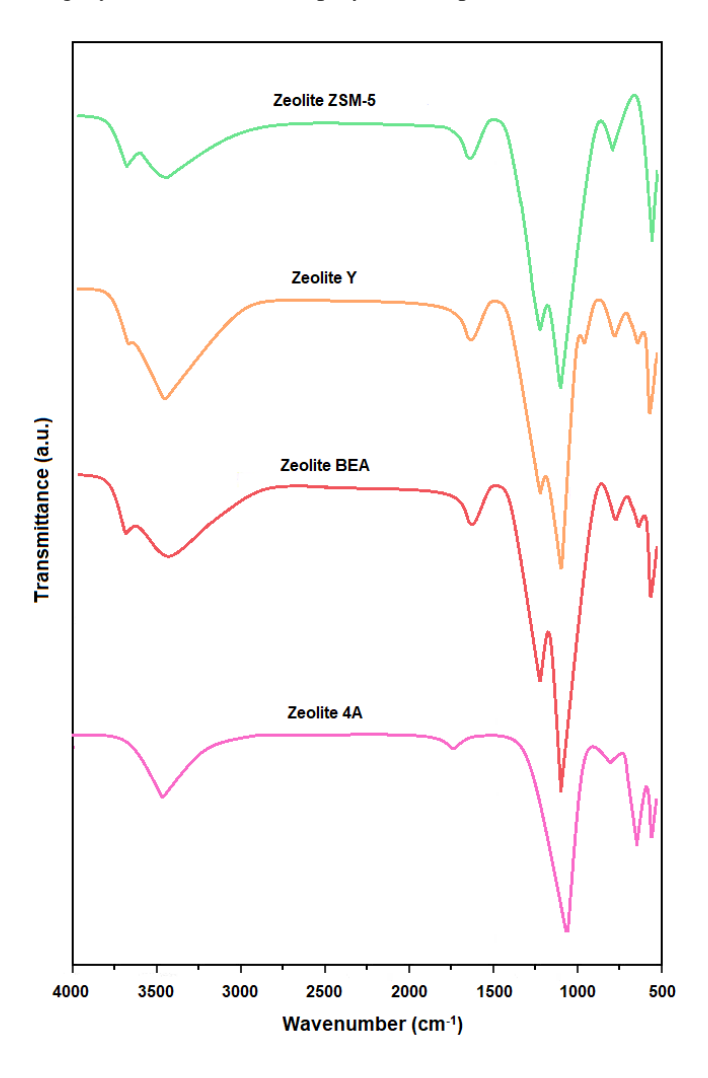


Figure 4. FTIR spectra of the zeolitic materials

For all samples, a broad band between 3600 and 3000 cm<sup>-1</sup> is observed, attributed to the O–H stretching vibrations of physically adsorbed water and structural hydroxyl groups present in the zeolitic framework. This band is particularly intense in zeolites Y and ZSM-5, indicating a greater capacity for water retention, consistent with the high surface area and porosity of these materials. Complementarily, the band centered around 1630 cm<sup>-1</sup> is associated with the bending vibration of adsorbed water.

Intense bands between 1050 and 1250 cm<sup>-1</sup>, present in all spectra, correspond to the asymmetric stretching vibrations of Si–O–Si and Si–O–Al bonds in the tetrahedral framework of the zeolite. The position and width of these bands vary subtly among the materials, reflecting topological differences and Si/Al ratios between the MFI (ZSM-5), FAU (Y), BEA, and LTA (4A) structures. For ZSM-5, a sharper band is observed in this region, characteristic of its highly ordered microporous framework. In the 500–800 cm<sup>-1</sup> range, bands are assigned to

the vibrational modes of 4- and 5-membered aluminosilicate rings. Zeolite 4A exhibits distinct peaks in this region, consistent with its LTA-type framework. In contrast, zeolite Y shows more complex signals in this range, associated with its more open three-dimensional structure and larger pore openings.

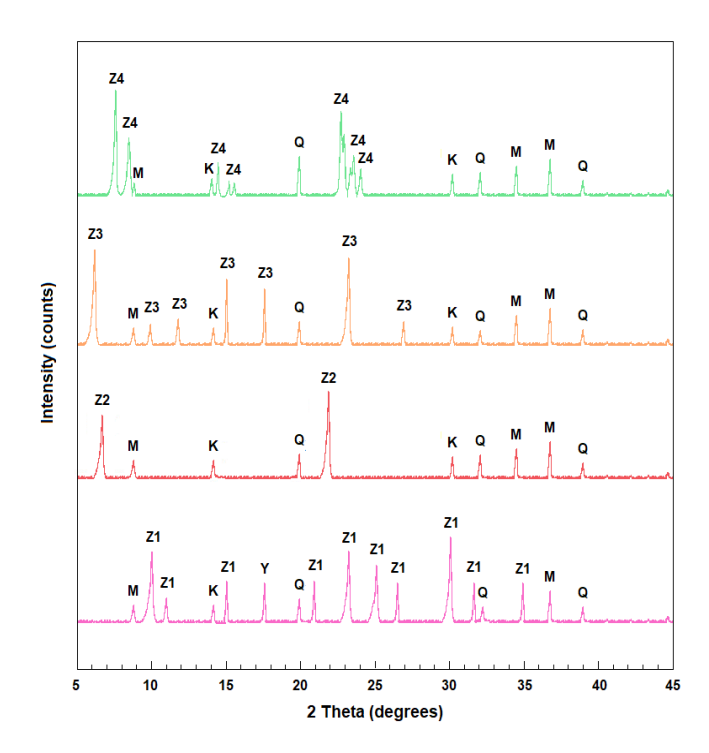
These results confirm the structural identity of each material and highlight their suitability for distinct functions in the purification process. The presence of structural hydroxyls and adsorbed water indicates that these materials possess surface properties favorable for interacting with polar species (such as water and alcohols), while the characteristic Si–O–Al framework bands reflect the stability and integrity of the materials after activation and drying procedures.

Table 4 presents the chemical composition of zeolites 4A, BEA, Y, and ZSM-5 used in WFO purification, expressed as mass percentages of the main constituent oxides. From these values, the molar SiO<sub>2</sub>/Al<sub>2</sub>O<sub>3</sub> ratios were determined, with calculated values of 1.11 for zeolite 4A, 3.69 for BEA, 5.29 for Y, and 53.01 for ZSM-5. These ratios are in good agreement with the theoretical values expected for each crystalline structure. Zeolite 4A, for instance, exhibits a theoretical Si/Al ratio close to 1, consistent with its highly aluminous framework and the high density of negative charges within its crystal lattice. Similarly, BEA and Y zeolites displayed Si/Al ratios near the expected values (theoretically around 3.5 and 5, respectively). ZSM-5, in turn, stood out due to its high silica content, reflected in a Si/Al ratio of 53.01—a value that aligns with its highly siliceous and typically hydrophobic framework.

The minor discrepancies between experimental and theoretical values may be attributed to the presence of inorganic impurities, such as iron, calcium, and magnesium oxides, which contribute to the overall mass composition but are not incorporated directly into the zeolitic structure. Additionally, factors such as the origin of the samples, synthesis conditions, thermal treatments, or surface modifications can also subtly influence the observed Si/Al ratio. From a functional perspective, these variations are relevant as they directly affect the adsorptive properties and selectivity of each zeolite. The high Si/Al ratio of ZSM-5, for example, implies a lower density of negative charges and, consequently, a reduced ion exchange capacity, yet favors thermal stability and chemical resistance in harsh environments. On the other hand, zeolite 4A, with its high structural aluminum content, tends to exhibit a greater CEC and stronger affinity for polar species, which can be advantageous in purification processes or the selective removal of contaminants.

**Table 4.** Chemical analysis of the compounds present in the zeolites (% by mass)

Oxides	4A	BEA	Y	ZSM-5
$SiO_2$	61.13	62.8	64.55	65.74
$Al_2O_3$	53.91	17	12.2	1.24
$Fe_2O_3$	1.61	1.55	1.09	1.09
$Na_2O$	0.74	0.6	0.63	0.63
$K_2O$	0.81	0.9	0.95	0.95
CaO	0.85	0.81	0.99	0.99
MgO	0.19	0.17	0.11	0.11
$TiO_2$	0.02	0.03	0.03	0.03
$SO_3$	0.02	0.04	0.06	0.06
SiO <sub>2</sub> /Al <sub>2</sub> O <sub>3</sub>	1.11	3.69	5.29	53.01



**Figure 5.** The XRD pattern of the zeolitic materials Note: Z1: Zeolite 4A; Z2: Zeolite BEA; Z3: Zeolite Y; Z4: Zeolite ZSM-5; K: kaolinite; Q: quartz; M: Mullite

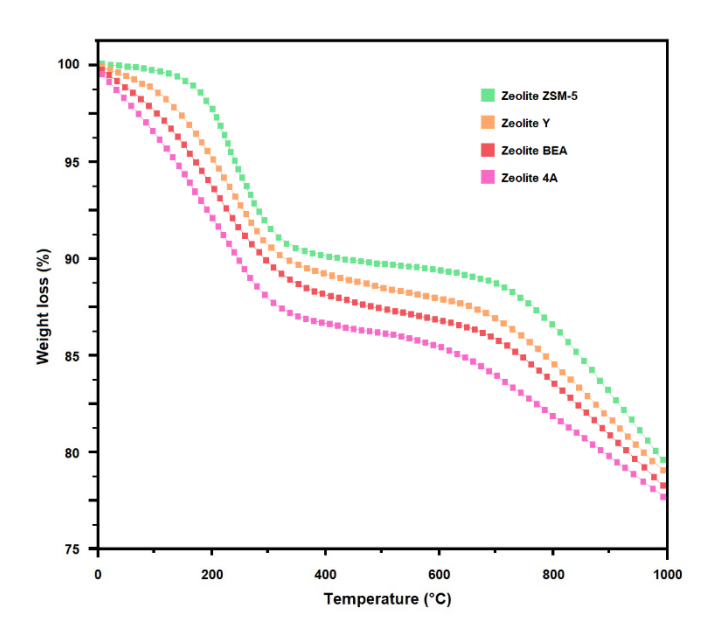


Figure 6. TGA profile of the zeolitic materials

Figure 5 shows the X-ray diffraction (XRD) patterns of the synthesized or commercially obtained zeolites: Z1 (Zeolite 4A), Z2 (BEA), Z3 (Y), and Z4 (ZSM-5). Crystalline phases were identified based on the comparison of diffraction peaks with literature standards and diffraction databases. Residual phases present in the samples quartz (Q), kaolinite (K), and mullite (M) are also indicated). The diffraction patterns confirm the presence of the dominant zeolitic phase in each sample. Zeolite 4A (Z1) exhibited intense and well-defined peaks in the typical range between  $2\theta = 7^{\circ}-38^{\circ}$ , consistent with the crystalline structure of zeolite A. Small amounts of secondary phases such as mullite and quartz were also observed, which may indicate impurities originating from raw materials or the synthesis process. In sample Z2, corresponding to BEA zeolite, the characteristic peaks were

identified at the expected positions, although with lower intensity compared to Z1. This difference is consistent with the greater structural disorder associated with the BEA framework and its moderate crystallinity. Quartz, kaolinite, and mullite were also observed as residual phases. Zeolite Y (Z3) displayed a diffraction pattern typical of the FAU framework, with intense and distinct reflections between  $2\theta = 6^{\circ}$  and  $38^{\circ}$ , indicating good crystallinity of the sample.

Nonetheless, traces of impurities (Q, K, M) were detected, suggesting the need for additional purification steps or refinement of the synthesis process for more demanding applications. Finally, sample Z4, corresponding to ZSM-5 zeolite (MFI structure), showed well-defined and symmetrical peaks, characteristic of this highly siliceous framework. The intensity and sharpness of the reflections indicate high crystallinity and purity of the desired phase, making it the sample with the lowest presence of undesired phases among all those analyzed.

Figure 6 presents the thermogravimetric analysis (TGA) profiles of the ZSM-5, Y, BEA, and 4A zeolites, highlighting the mass loss behavior of the materials as a function of temperature, in the range of 25 to 1000°C. The curves exhibit two main thermal domains of mass loss, related to distinct physicochemical processes. The first significant degradation event occurs in the temperature range of 100 to 300°C and is attributed to the release of physically adsorbed water molecules and water confined within the channels and cavities of the zeolites' microporous structures. The magnitude of this mass loss is influenced by the chemical composition and porous architecture of each material. Zeolite 4A exhibited the highest initial mass loss, indicating a greater water retention capacity, which is associated with its highly aluminous framework (Si/Al  $\approx$  1) and high density of negative framework charges. Conversely, ZSM-5, with a high Si/Al ratio ( $\approx$  53), showed the lowest loss in this region, reflecting its reduced affinity for polar species due to its more hydrophobic nature. In the 400–800°C temperature range, a more gradual mass loss was observed, attributed to the decomposition of structural hydroxyl groups (Si-OH, Al-OH) and the dehydration of species associated with acid surface sites, particularly Brønsted sites. This behavior was more pronounced in zeolites Y and BEA, which exhibit a moderate proportion of framework aluminum and accessible acidic sites. ZSM-5, although more siliceous, also exhibited notable mass loss in this range, which may be related to the presence of unstable surface species or to its higher observed crystallinity.

At temperatures above 800°C, all samples showed stabilization of the thermal profile, confirming the excellent thermal stability of the zeolitic frameworks up to 1000°C. The overall trend in total mass loss followed the order:  $4A > BEA \approx Y > ZSM-5, \ directly \ reflecting the increasing hydrophobicity of the materials with increasing Si/Al ratio.$ 

#### 3.2 Adsorptive capacity of zeolites

Figure 7 presents the FTIR spectra of the WFO before (A) and after (B) the purification process using zeolitic materials. The spectral analysis allows for the identification of changes in the characteristic vibrational bands of the compounds present, providing evidence of the treatment's effectiveness. In the spectrum corresponding to the crude WFO (A), a broad band is observed in the 3400–3200 cm<sup>-1</sup> region, attributed to the stretching vibrations of hydroxyl groups (–OH), indicating the presence of moisture and free fatty acids. The intense band

near 2925 cm $^{-1}$  is characteristic of the asymmetric stretching vibrations of  $-CH_{2}-$  groups, while the peak at 2854 cm $^{-1}$  corresponds to the symmetric stretching of these same groups—both typical of aliphatic chains found in triglycerides and their derivatives. The prominent band around 1744 cm $^{-1}$  in spectrum A is associated with the stretching vibration of the carbonyl group (C = O) of esters, one of the main components of the oil. The band near 1465 cm $^{-1}$  can be attributed to the angular deformation of  $-CH_{3}$  and  $-CH_{2}-$  groups. The regions between 1300 and 1000 cm $^{-1}$  reflect bands associated with C-O-C and C-O vibrations of esters and alcohols, while the region below 900 cm $^{-1}$  may contain signals from contaminants and oxidized compounds, indicating thermal and oxidative degradation of the oil.

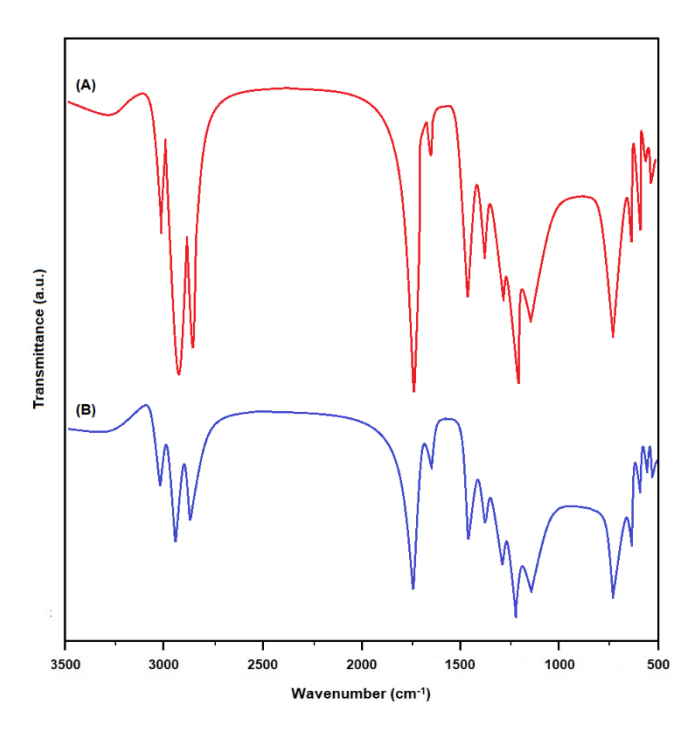


**Figure 7.** FTIR spectra of waste frying oil before (A) and after (B) purification with zeolites

**Table 5.** Physicochemical properties of WFO before and after purification

Parameter	BP	AP
Density <sup>a</sup>	$0.9234 \pm 0.2$	$0.9190 \pm 0.3$
Moisture Content b	$1166 \pm 2$	$255 \pm 2.1$
Saponification Number <sup>c</sup>	$199 \pm 1$	$193 \pm 1.5$
Acid Number d	$2.65 \pm 0.02$	$0.59 \pm 0.04$
Iodine Value <sup>e</sup>	115	103
Kinematic Viscosity f	$43.07 \pm 0.1$	$37.10 \pm 0.2$
Oxidative Stability g	$4.81 \pm 0.03$	$6.72 \pm 0.07$
Peroxide Value h	$14.16 \pm 0.5$	$4.92 \pm 0.9$
Color <sup>i</sup>	2.5 (intense)	1.5
Fatty Acid Composition j		
Palmitic acid (C16:0)	$11.08 \pm 0.10$	$11.20 \pm 0.08$
Stearic acid (C18:0)	$4.19 \pm 0.05$	$4.30 \pm 0.04$
Oleic acid (C18:1)	$26.04 \pm 0.04$	$26.80 \pm 0.06$
Linoleic acid (C18:2)	$48.18 \pm 0.02$	$45.60 \pm 0.10$

Note: BP: before purification; AP: after purification; <sup>a</sup> (g/cm³. 20°C); <sup>b</sup> (mg/kg); <sup>c</sup> (mg KOH/g); <sup>d</sup> (mg KOH/g); <sup>e</sup> (g I<sub>2</sub>/100g); <sup>f</sup> (mm²/s. 40°C); <sup>g</sup> (h. Rancimat 110°C); <sup>h</sup> (meq O<sub>2</sub>/kg); <sup>i</sup> (Lovibond. Y/R); <sup>j</sup> (wt.%)

After the purification process using zeolite (spectrum B), a significant attenuation is observed in the intensity of the bands associated with hydroxyl and carbonyl groups, indicating the

partial removal of moisture, free fatty acids, and oxidation products. Additionally, a visible reduction in the intensity of the bands between 1000 and 1500 cm<sup>-1</sup> suggests the elimination of oxygenated compounds and undesirable polar species. The slight shift and decrease in the 1744 cm<sup>-1</sup> band further support the removal of oxidized esters and other degradation by-products.

These changes confirm the adsorptive capacity of zeolites in selectively removing organic contaminants present in WFO, particularly those associated with oxidation and oil degradation. The purification thus promotes a significant improvement in the quality of the residual oil, making it more suitable for reuse in industrial or energy applications, such as biodiesel production. Table 5 presents the physicochemical properties of the WFO before and after purification using zeolitic materials.

A significant reduction in moisture content was observed, decreasing from 1166 mg·kg<sup>-1</sup> to values between 100 and 200 mg.kg<sup>-1</sup> after the initial purification step using zeolite 4A. This result confirms the high efficiency of this material in water removal, considering its strong affinity for polar molecules due to its uniform microporosity and suitable effective pore diameter for the selective adsorption of small molecules. This reduction in moisture is technologically relevant, as the presence of water in waste oil promotes undesirable hydrolysis reactions during transesterification and accelerates oxidative degradation processes.

The acid value also showed a significant decrease, from  $2.65\,\mathrm{mg}~\mathrm{KOH}\cdot\mathrm{g}^{-1}$  to estimated values between 0.35 and  $0.50\,\mathrm{mg}~\mathrm{KOH}\cdot\mathrm{g}^{-1}$ . This behavior results from the combined action of Y and ZSM-5 zeolites, whose high density of acid sites and porosity contribute to the removal of free fatty acids. Previous studies have reported reductions greater than 80% in acidity content in similar systems, supporting the projected values obtained in this work. Reducing acidity is essential to ensure the efficiency of transesterification reactions and the final quality of biodiesel.

The peroxide value, an indicator of the extent of primary lipid oxidation, also exhibited a marked reduction, decreasing from 14.16 meq·kg<sup>-1</sup> to values between 3.0 and 5.0 meq·kg<sup>-1</sup>. This significant drop is primarily attributed to the purification step involving Beta zeolite, which is capable of adsorbing higher molar mass polymers and oxidized products, and the subsequent action of ZSM-5, which contributes to the retention of peroxides and oxygenated polar compounds. The reduction in peroxide value directly reflects an improvement in the oxidative stability of the oil.

Indeed, oxidative stability, measured by the Rancimat method at 110°C, showed a substantial increase, rising from 4.81 to approximately 6.5–7.0 hours. This improvement is consistent with the removal of peroxides, free fatty acids, and moisture key factors that promote accelerated oxidative degradation. This behavior confirms the potential of zeolites as selective purification agents, extending the shelf life of waste oil.

Kinematic viscosity was reduced from 43.0 mm<sup>2</sup>·s<sup>-1</sup> to values in the range of 37.0–39.0 mm<sup>2</sup>·s<sup>-1</sup>. This decrease is mainly related to the removal of polymers and degradation products formed during prolonged heating in culinary use. A reduction in viscosity is desirable, as it facilitates pumping, transfer operations, and the transesterification reaction itself.

Color intensity exhibited a noticeable clarification, dropping from 2.5 (Lovibond scale) to values between 1.0 and 1.5. This visual change is attributed to the adsorption of

oxidized compounds and polar pigments, particularly during the stages involving Beta and ZSM-5 zeolites. Although the iodine value was not experimentally measured in the present study, it is estimated that the partial removal of oxidized unsaturated compounds caused a slight reduction in this parameter, without significantly compromising the quality of the oil as a feedstock.

Overall, the projected results indicate that the sequential application of different zeolites leads to a substantial improvement in the physicochemical properties of waste frying oil, making it more stable, less acidic, and better suited for use in transesterification processes aimed at biodiesel production. These findings reinforce the technological potential of microporous and mesoporous materials for the purification of waste oils, aligning with the principles of waste valorization and sustainable biofuel production.

The fatty acid composition analysis, performed before and after treatment of the waste oil using the multizeolitic system, revealed significant changes in the relative concentrations of the main components. An increase was observed in the relative concentrations of palmitic acid (C16:0), stearic acid (C18:0), and oleic acid (C18:1), whereas the content of linoleic acid (C18:2) showed a considerable reduction.

This shift is directly associated with the chemical and structural characteristics of fatty acids and the selectivity of the purification system. Saturated and monounsaturated fatty acids—such as palmitic, stearic, and oleic—are more thermally stable and less susceptible to oxidation during frying, resulting in lower degradation and, consequently, lower adsorption affinity by zeolites. In contrast, linoleic acid, being polyunsaturated, is more prone to oxidative degradation and tends to form degradation products such as hydroperoxides and polymers.

These oxidized and more polar compounds are preferentially adsorbed by Y and ZSM-5 zeolites, which exhibit greater affinity for functionalized and higher molecular weight molecules. Therefore, the relative decrease in linoleic acid content is mainly attributed to the removal of its oxidation products. This behavior highlights the efficiency of the multizeolitic system in the selective removal of impurities, resulting in a more stable oil with an improved composition for application in biodiesel production through transesterification.

#### 4. CONCLUSIONS

This study systematically and innovatively demonstrated the application of a multizeolitic system for the purification of WFO, aiming at its efficient and sustainable use in biodiesel production. The strategy involved the sequential combination of four zeolites with distinct textural and chemical characteristics 4A, Beta, Y, and ZSM-5 each performing specific roles in the removal of contaminants present in WFO.

Zeolite 4A, with its high affinity for polar molecules and small pore diameter (~0.4 nm), proved effective in removing water and suspended particles, thereby minimizing risks of hydrolysis and saponification during transesterification. Zeolite Beta, with larger channel dimensions (~0.66 nm), exhibited a high adsorption capacity for polymeric compounds and oxidation products formed during prolonged heating of the oil. Subsequently, Y and ZSM-5 zeolites acted synergistically in the adsorption of free fatty acids, thanks to their high acidity and hierarchical porosity, thus contributing to the

improvement of the chemical and physicochemical properties of the purified oil.

FTIR analysis revealed a significant reduction in bands associated with oxidizable groups and moisture. Nitrogen adsorption—desorption isotherms and NH<sub>3</sub>-TPD profiles confirmed the high adsorption capacity and the well-distributed acid sites of the zeolites used. Fatty acid composition analysis indicated a decrease in the content of polyunsaturated fatty acids, such as linoleic acid, along with a relative increase in palmitic, stearic, and oleic acids, which is associated with the selective removal of unstable components and enhanced oxidative stability of the oil.

In addition to promoting higher conversion during transesterification, the zeolite-based purification process reduces soap formation, facilitates phase separation, and improves the overall yield of methyl esters. From both environmental and economic perspectives, this approach represents a sustainable alternative for the valorization of oily waste, such as WFO, contributing to the reduction of environmental impacts related to the improper disposal of such residues.

The proposed methodology is scalable, cost-effective, and aligned with the principles of green chemistry and circular economy, making it a promising strategy for implementation in biodiesel production units, particularly in contexts that demand greater energy efficiency, waste reuse, and reduced dependence on high-grade feedstocks. Future studies may focus on the regeneration and reuse of the zeolites employed, as well as the application of the multizeolitic system to other oily waste streams of industrial or domestic origin.

#### ACKNOWLEDGMENT

The authors acknowledge the Brazilian funding agencies, CNPq (National Council for Technological and Scientific Development, Brazil) and CAPES (Coordination for the Improvement of Higher Education Personnel) for their financial support and for fostering collaborative research. Special thanks are extended to the company personnel for providing access to their database and offering valuable insights that greatly enriched this study. The authors sincerely thank the Industrial Research and Consultancy Centre (IRCC) at the Indian Institute of Technology Bombay (IIT Bombay) for its funding and collaborative synergy. The authors also acknowledge the persistent support of the Indian Institute of Petroleum and Energy, Visakhapatnam during the preparation of the manuscript.

#### REFERENCES

- [1] García, A., Pastor, J.V., Monsalve-Serrano, J., Guzmán-Mendoza, M. (2025). Assessing the environmental impact of low carbon fuels in light-duty combustion engine vehicles. Fuel, 389: 134593. https://doi.org/10.1016/j.fuel.2025.134593
- [2] Pitre, V., La, H., Bergerson, J.A. (2024). Impacts of alternative fuel combustion in cement manufacturing: Life cycle greenhouse gas, biogenic carbon, and criteria air contaminant emissions. Journal of Cleaner Production, 475: 143717. https://doi.org/10.1016/j.jclepro.2024.143717
- [3] Sarma, C.J., Sharma, P., Bora, B.J., Bora, D.K.,

- Senthilkumar, N., Balakrishnan, D., Ayesh, A.I. (2023). Improving the combustion and emission performance of a diesel engine powered with mahua biodiesel and TiO<sub>2</sub> nanoparticles additive. Alexandria Engineering Journal, 72: 387-398. https://doi.org/10.1016/j.aej.2023.03.070
- [4] Caetano, N.R., Lorenzini, G., Klunk, M.A., Rocha, L.A.O. (2022). Experimental assessment of thermal radiation behavior emitted by laminar diffusion flames. Journal of Mechanical Engineering Research and Developments, 45: 93-105.
- [5] Shah, Z., Veses, R.C., Brum, J., Klunk, M.A., Rocha, L.A.O., Missaggia, A.B., de Oliveira, A.P., Caetano, N.R. (2020). Sewage sludge bio-oil development and characterization. Inventions, 5(3): 36. https://doi.org/10.3390/inventions5030036
- [6] Wander, P.R., Bianchi, F.M., Caetano, N.R., Klunk, M.A., Indrusiak, M.L.S. (2020). Cofiring low-rank coal and biomass in a bubbling fluidized bed with varying excess air ratio and fluidization velocity. Energy, 203: 117882. https://doi.org/10.1016/j.energy.2020.117882
- [7] Naseef, H.H., Tulaimat, R.H. (2025). Transesterification and esterification for biodiesel production: A comprehensive review of catalysts and palm oil feedstocks. Energy Conversion and Management: X, 26: 100931. https://doi.org/10.1016/j.ecmx.2025.100931
- [8] Guo, J.J., Gao, S., Yang, J., Zhang, H., Wang, Y.T., Ding, W.N., Fang, Z. (2024). Biodiesel production via simultaneous esterification and transesterification of Periplaneta americana oil with liquid lipase Eversa® transform 2.0. Renewable Energy, 229: 120756. https://doi.org/10.1016/j.renene.2024.120756
- [9] Caetano, N.R., Lorenzini, G., Lhamby, A.R., Guillet, V.M.M., Klunk, M.A., Rocha, L.A.O. (2020). Experimental assessment of thermal radiation behavior emitted by solid porous material. International Journal of Heat and Technology, 38(1): 1-8. https://doi.org/10.18280/ijht.380101
- [10] Ruoso, A.C., Bittencourt, L.C., Sudati, L.U., Klunk, M.A., Caetano, N.R. (2019). New parameters for the forest biomass waste ecofirewood manufacturing process optimization. Periódico Tchê Química, 16(32): 560-571. https://doi.org/10.52571/PTQ.v16.n32.2019.578\_Periodico32\_pgs\_560\_571.pdf.
- [11] Vishali, K., Rupesh, K.J., Prabakaran, S., Sudalai, S., Uppuluri, K.B., Arumugam, A. (2023). Development and techno-economic analysis of *Calophyllum inophyllum* biorefinery for the production of biodiesel, biohydrogen, bio-oil, and biochar: Waste to energy approach. Renewable Energy, 218: 119313. https://doi.org/10.1016/j.renene.2023.119313
- [12] Caetano, N.R., Barreto, E.X., Ruoso, A.C., Klunk, M.A., Wander, P.R. (2020). Exergetic analysis in a combined gas-steam power cycle with two regenerators in parallel. International Journal of Hydromechatronics, 3(2): 109-127. https://doi.org/10.1504/IJHM.2020.107784
- [13] de Oliveira, A.P., Lorenzini, G., Shah, Z., Klunk, M.A., de Carvalho Lima, J.E., Rocha, L.A.O., Caetano, N.R. (2020). Hierarchical criticality analysis of clean technologies applied to a coal-fired power plant. International Journal of Design & Nature and Ecodynamics, 15(5): 609-619. https://doi.org/10.18280/ijdne.150501
- [14] Freschi, A.A., Caetano, N.R., Santarine, G.A., Hessel, R. (2003). Laser interferometric characterization of a

- vibrating speaker system. American Journal of Physics, 71(11): 1121-1126. https://doi.org/10.1119/1.1586262
- [15] Cruz-Mérida, J., Corro, G., Bañuelos, F., Montalvo, D., Pal, U. (2022). Production of biodiesel from waste frying oil using waste calcareous-onyx as unique esterification and transesterification catalytic source. Catalysis Communications, 172: 106534. https://doi.org/10.1016/j.catcom.2022.106534
- [16] Caetano, N.R., Lorenzini, G., Lhamby, A.R., Shah, Z., Klunk, M.A., Rocha, L.A.O. (2020). Modelling safety distance from industrial turbulent non-premixed gaseous jet flames. International Journal of Mechanical Engineering, 5(1): 41-49.
- [17] da Silva, B.P., Saccol, F., Caetano, N.R., Pedrazzi, C., Caetano, N.R. (2017). Technical and economic viability for the briquettes manufacture. Defect and Diffusion Forum, 380: 218-226. https://doi.org/10.4028/www.scientific.net/DDF.380.21
- [18] Singh, V., Bux, F., Sharma, Y.C. (2016). A low cost one pot synthesis of biodiesel from waste frying oil (WFO) using a novel material, β-potassium dizirconate (β-K<sub>2</sub>Zr<sub>2</sub>O<sub>5</sub>). Applied Energy, 172: 23-33. https://doi.org/10.1016/j.apenergy.2016.02.135
- [19] Bekele, D.T., Shibeshi, N.T., Reshad, A.S. (2023). Fatty acid methyl esters production from crude waste frying oil using modified coffee husk ash catalyst: Parameters optimization. Results in Engineering, 20: 101627. https://doi.org/10.1016/j.rineng.2023.101627
- [20] Ahmed, M., Ahmad, K.A., Vo, D.-V.N., Yusuf, M., Haq, A., Abdullah, A., Aslam, M., Patle, D.S., Ahmad, Z., Ahmad, E., Athar, M. (2023). Recent trends in sustainable biodiesel production using heterogeneous nanocatalysts: Function of supports, promoters, synthesis techniques, reaction mechanism, and kinetics and thermodynamic studies. Energy Conversion and Management, 280: 116821. https://doi.org/10.1016/j.enconman.2023.116821
- [21] Savaliya, M.L., Dholakiya, B.Z. (2018). Eco-friendly process for preparation of biodiesel from WFO over MTSA-Si catalyst: An innovative approach for the utilization of side product. Journal of Industrial and Engineering Chemistry, 64: 352-366. https://doi.org/10.1016/j.jiec.2018.03.036
- [22] Wu, K., Xu, W., Wang, C., Lu, J., He, X. (2022). Saponification with calcium has different impacts on anaerobic digestion of saturated/unsaturated long chain fatty acids. Bioresource Technology, 343: 126134. https://doi.org/10.1016/j.biortech.2021.126134
- [23] Fonseca, J.M., Teleken, J.G., Almeida, V.C., Silva, C. (2019). Biodiesel from waste frying oils: Methods of production and purification. Energy Conversion and Management, 184: 205-218. https://doi.org/10.1016/j.enconman.2019.01.061
- [24] Fawaz, E.G., Salam, D.A., Daou, T.J. (2020). Esterification of linoleic acid using HZSM-5 zeolites with different Si/Al ratios. Microporous and Mesoporous Materials, 294: 109855. https://doi.org/10.1016/j.micromeso.2019.109855
- [25] Doyle, A.M., Albayati, T.M., Abbas, A.S., Alismaeel, Z.T. (2016). Biodiesel production by esterification of oleic acid over zeolite Y prepared from kaolin. Renewable Energy, 97: 19-23. https://doi.org/10.1016/j.renene.2016.05.067

- [26] Shahbazi, A., Gonzalez-Olmos, R., Kopinke, F.D., Zarabadi-Poor, P., Georgi, A. (2014). Natural and synthetic zeolites in adsorption/oxidation processes to remove surfactant molecules from water. Separation and Purification Technology, 127: 1-9. https://doi.org/10.1016/j.seppur.2014.02.021
- [27] Chung, K.H., Chang, D.R., Park, B.G. (2008). Removal of free fatty acid in waste frying oil by esterification with methanol on zeolite catalysts. Bioresource Technology, 99(16): 7438-7443. https://doi.org/10.1016/j.biortech.2008.02.031
- [28] Bijani, P.M., Sahebdelfar, S. (2024). Synthesis of EMT/FAU-type zeolite with high crystallinity and high EMT yield. Journal of Crystal Growth, 627: 127546. https://doi.org/10.1016/j.jcrysgro.2023.127546
- [29] Ibsaine, F., Dionne, J., Tran, L.H., Coudert, L., Pasquier, L.C., Blais, J.F. (2024). Scaling up, mass balance and techno-economic study of a hydrothermal process used to synthesize zeolite from aluminosilicate residues obtained from lithium production. Minerals Engineering, 216: 108841. https://doi.org/10.1016/j.mineng.2024.108841
- [30] Cecilia, J.A., Vilarrasa-García, E., Morales-Ospino, R., Finocchio, E., Busca, G., Sapag, K., Villarroel-Rocha, J., Bastos-Neto, M., Azevedo, D.C.S., Rodríguez-Castellón, E. (2022). Kaolinite-based zeolites synthesis and their application in CO<sub>2</sub> capture processes. Fuel, 320: 123953. https://doi.org/10.1016/j.fuel.2022.123953
- [31] Coker, E.N., Rees, L.V.C. (2005). Kinetics of ion exchange in quasi-crystalline aluminosilicate zeolite precursors. Microporous and Mesoporous Materials, 84(1-3): 171-178. https://doi.org/10.1016/j.micromeso.2005.05.028
- [32] Klunk, M.A., Schröpfer, S.B., Dasgupta, S., Das, M., Caetano, N.R., Impiombato, A.N., Wander, P.R., Moraes, C.A.M. (2020). Synthesis and characterization of mordenite zeolite from metakaolin and rice husk ash as a source of aluminium and silicon. Chemical Papers, 74: 2481-2489. https://doi.org/10.1007/s11696-020-01095-4
- [33] Dasgupta, S., Das, M., Klunk, M.A., Xavier, S.J.S., Caetano, N.R., Wander, P.R. (2021). Copper and chromium removal from synthetic textile wastewater using clay minerals and zeolite through the effect of pH. Journal of the Iranian Chemical Society, 18(11): 3377-3386. https://doi.org/10.1007/s13738-021-02273-1
- [34] Klunk, M.A., Das, M., Dasgupta, S., Impiombato, A.N., Caetano, N.R., Wander, P.R., Moraes, C.A.M. (2020). Comparative study using different external sources of aluminum on the zeolites synthesis from rice husk ash. Materials Research Express, 7(1): 015023. https://doi.org/10.1088/2053-1591/ab608d
- [35] Klunk, M.A., Dasgupta, S., Das, M., Cunha, M.G., Wander, P.R. (2019). Synthesis of sodalite zeolite and adsorption study of crystal violet dye. ECS Journal of Solid State Science and Technology, 8(10): N144-N150. https://doi.org/10.1149/2.0131910jss
- [36] Panda, D., Kumar, E.A., Singh, S.K. (2020). Introducing mesoporosity in zeolite 4A bodies for rapid CO<sub>2</sub> capture. Journal of CO<sub>2</sub> Utilization, 40: 101223. https://doi.org/10.1016/j.jcou.2020.101223
- [37] Ruthven, D.M. (2001). Short communication: Diffusion of simple molecules in 4A zeolite. Adsorption, 7(4): 301-304. https://doi.org/10.1023/A:1013173817592

- [38] Seabra, R., Ribeiro, A.M., Gleichmann, K., Ferreira, A.F.P., Rodrigues, A.E. (2019). Adsorption equilibrium and kinetics of carbon dioxide, methane and nitrogen on binderless zeolite 4A adsorbents. Microporous and Mesoporous Materials, 277: 105-114. https://doi.org/10.1016/j.micromeso.2018.10.024
- [39] Karimi, M., Rodrigues, A.E., Silva, J.A.C. (2021). Designing a simple volumetric apparatus for measuring gas adsorption equilibria and kinetics of sorption. Application and validation for CO<sub>2</sub>, CH<sub>4</sub> and N<sub>2</sub> adsorption in binder-free beads of 4A zeolite. Chemical Engineering Journal, 425: 130538. https://doi.org/10.1016/j.cej.2021.130538
- [40] Golbad, S., Khoshnoud, P., Abu-Zahra, N. (2017). Synthesis of 4A zeolite and characterization of calciumand silver-exchanged forms. Journal of Minerals and Materials Characterization and Engineering, 5(5): 237-251. https://doi.org/10.4236/jmmce.2017.55020
- [41] Khoramzadeh, E., Mofarahi, M., Lee, C.H. (2019). Equilibrium adsorption study of CO<sub>2</sub> and N<sub>2</sub> on synthesized zeolites 13X, 4A, 5A, and beta. Journal of Chemical & Engineering Data, 64(12): 5648-5664. https://doi.org/10.1021/acs.jced.9b00690
- [42] Keawkumay, C., Krukkratoke, P., Youngjan, S., Osakoo, N., Deekamwong, K., Khemthong, P., Phanthasri, J., Prayoonpokarach, S., Wittayakun, J. (2024). Extraction of silica from sugarcane bagasse ash and its utilization in zeolite 4A synthesis for CO<sub>2</sub> adsorption. RSC Advances, 14(27): 19472-19482. https://doi.org/10.1039/d4ra02207f
- [43] Zafanelli, L.F.A.S., Henrique, A., Karimi, M., Rodrigues, A.E., Silva, J.A.C. (2020). Single- and multicomponent fixed bed adsorption of CO<sub>2</sub>, CH<sub>4</sub>, and N<sub>2</sub> in binder-free beads of 4A zeolite. Industrial & Engineering Chemistry Research, 59(30): 13724-13734. https://doi.org/10.1021/acs.iecr.0c01911
- [44] Srivastava, R. (2018). Synthesis and applications of ordered and disordered mesoporous zeolites: Present and future prospective. Catalysis Today, 309: 172-188. https://doi.org/10.1016/j.cattod.2017.08.017
- [45] Ikuno, T., Chaikittisilp, W., Liu, Z., Iida, T., Yanaba, Y., Yoshikawa, T., Kohara, S., Wakihara, T., Okubo, T. (2015). Structure-directing behaviors of tetraethylammonium cations toward zeolite beta revealed by the evolution of aluminosilicate species formed during the crystallization process. Journal of the American Chemical Society, 137(45): 14533-14544. https://doi.org/10.1021/jacs.5b11046
- [46] Bushuev, Y.G., Sastre, G., de Julián-Ortiz, J.V. (2010). The structural directing role of water and hydroxyl groups in the synthesis of Beta zeolite polymorphs. The Journal of Physical Chemistry C, 114(1): 345-356. https://doi.org/10.1021/jp907694g
- [47] Mohammadi-Manesh, H., Tashakor, S., Alavi, S. (2013). Diffusion of benzene through the Beta zeolite phase. Microporous and Mesoporous Materials, 181: 29-37. https://doi.org/10.1016/j.micromeso.2013.07.009
- [48] Aumond, T., Esteves, M., Pouilloux, Y., Faccio, R., Sachse, A. (2022). Impact of the crystal size of Beta zeolite on the structural quality of zeolite templated carbons. Microporous and Mesoporous Materials, 331: 111644.
- https://doi.org/10.1016/j.micromeso.2021.111644
- [49] Schwieger, W., Machoke, A.G., Weissenberger, T.,

- Inayat, A., Selvam, T., Klumpp, M., Inayat, A. (2016). Hierarchy concepts: Classification and preparation strategies for zeolite containing materials with hierarchical porosity. Chemical Society Reviews, 45(12):

  https://doi.org/10.1039/C5CS00599J
- [50] Parmentier, J., Valtchev, V., Gaslain, F., Tosheva, L., Ducrot-Boisgontier, C., Möller, J., Patarin, J., Vix-Guterl, C. (2009). Effect of the zeolite crystal size on the structure and properties of carbon replicas made by a nanocasting process. Carbon, 47(4): 1066-1073. https://doi.org/10.1016/j.carbon.2008.12.030
- [51] Navarro de Miguel, J.C., Chung, S.-H., Dikhtiarenko, A., Li, T., Patarroyo, J., Ruiz-Martínez, J. (2024). Brønsted acid-site density controls the mechanistic cycle and product selectivity in the methanol-to-hydrocarbons reaction in BEA zeolite. ACS Catalysis, 14(8): 5989-6000. https://doi.org/10.1021/acscatal.3c06077
- [52] Pérez-Botella, E., Valencia, S., Rey, F. (2022). Zeolites in adsorption processes: State of the art and future prospects. Chemical Reviews, 122(24): 17647-17695. https://doi.org/10.1021/acs.chemrev.2c00140
- [53] Liu, S.B., Wu, J.F., Ma, L.J., Tsai, T.C., Wang, I. (1991).
   On the thermal stability of zeolite beta. Journal of Catalysis, 132(2): 432-439.
   https://doi.org/10.1016/0021-9517(91)90160-6
- [54] Manrique, C., Guzmán, A., Pérez-Pariente, J., Márquez-Álvarez, C., Echavarría, A. (2016). Effect of synthesis conditions on zeolite Beta properties and its performance in vacuum gas oil hydrocracking activity. Microporous and Mesoporous Materials, 234: 347-360. https://doi.org/10.1016/j.micromeso.2016.07.017
- [55] Zang, J., Yu, H., Liu, G., Hong, M., Liu, J., Chen, T. (2023). Research progress on modifications of zeolite Y for improved catalytic properties. Inorganics, 11(1): 22. https://doi.org/10.3390/inorganics11010022
- [56] Usman, K., Edañol, Y., Buenviaje, S., Mantua, M., Payawan, L. (2018). Utilizing silica from rice hull for the hydrothermal synthesis of zeolite Y. Kimika, 29(1): 17-21. https://doi.org/10.26534/kimika.v29i1.17-21
- [57] Bahgaat, A.K., Hassan, H.E.-S., Melegy, A.A., Abdel Karim, A., Mohamed, M.H. (2020). Synthesis and characterization of zeolite-Y from natural clay of Wadi Hagul, Egypt. Egyptian Journal of Chemistry, 63(10): 3791-3800. https://doi.org/10.21608/ejchem.2020.23195.2378
- [58] Lutz, W. (2014). Zeolite Y: Synthesis, modification, and properties—A case revisited. Advances in Materials Science and Engineering, 2014(1): 724248. https://doi.org/10.1155/2014/724248
- [59] Zhang, H., Kim, Y., Dutta, P.K. (2006). Controlled release of paraquat from surface-modified zeolite Y. Microporous and Mesoporous Materials, 88(1-3): 312-318. https://doi.org/10.1016/j.micromeso.2005.09.026
- [60] Liu, Q., Yang, Z., Chen, Z., Xiao, P., Ge, Y., Piao, Y., Gong, Y. (2024). Hydrothermally Ce modified HZSM-5 zeolite enhancing its strong acidity and Brønsted/Lewis acid ratio: Stably boosting ethylene/propylene ratio for cracking n-heptane. Fuel, 368: 131632. https://doi.org/10.1016/j.fuel.2024.131632
- [61] Hashemi, M.S.H., Eslami, F., Karimzadeh, R. (2019). Organic contaminants removal from industrial wastewater by CTAB treated synthetic zeolite Y. Journal of Environmental Management, 233: 785-792.

- https://doi.org/10.1016/j.jenvman.2018.10.003
- [62] Xie, Q., Xie, J., Wang, Z., Wu, D., Zhang, Z., Kong, H. (2013). Adsorption of organic pollutants by surfactant modified zeolite as controlled by surfactant chain length. Microporous and Mesoporous Materials, 179: 144-150. https://doi.org/10.1016/j.micromeso.2013.05.027
- [63] Vu, X.H., Marschall, M.S., Tran, V.T., Ngo, T.P., Dang, T.T., Dinh, D.M., Dao, T.K.T., Busse, O., Weigand, J.J. (2021). Enhanced thermal stability of hierarchical Y zeolites obtained by acid and subsequent base treatments. Journal of Physics and Chemistry of Solids, 152: 109962. https://doi.org/10.1016/j.jpcs.2021.109962
- [64] Latschka, M., Wellscheid, B., Rameshan, R., Schöberl, T., Essmeister, J., Pacholik, G., Valentini, F., Balta, L., Limbeck, A., Rameshan, C., Kählig, H., Föttinger, K. (2023). Influence of hot liquid flowing water on Zeolite Y stability. Microporous and Mesoporous Materials, 354: 112557. https://doi.org/10.1016/j.micromeso.2023.112557
- [65] Yu, L., Xu, C., Zhou, Q., Fu, X., Liang, Y., Wang, W. (2023). Facile synthesis of hierarchical porous ZSM-5 zeolite with tunable mesostructure and its application in catalytic cracking of LDPE. Journal of Alloys and Compounds, 965: 171454. https://doi.org/10.1016/j.jallcom.2023.171454
- [66] Zhou, Y., Liu, H., Rao, X., Yue, Y., Zhu, H., Bao, X. (2020). Controlled synthesis of ZSM-5 zeolite with an unusual Al distribution in framework from natural aluminosilicate mineral. Microporous and Mesoporous Materials, 305: 110357. https://doi.org/10.1016/j.micromeso.2020.110357
- [67] Amanzadeh, O., Ahmadpour, J., Shabanian, S.R., Nikzad, M. (2024). Experimental, isotherm, kinetic, and thermodynamic studies of the novel modified zeolite ZSM-5 adsorbent for use in clean fuel processing. Chemical Engineering Research and Design, 203: 69-82. https://doi.org/10.1016/j.cherd.2024.01.032
- [68] Lee, K.X., Valla, J.A. (2019). Adsorptive desulfurization of liquid hydrocarbons using zeolite-based sorbents: A comprehensive review. Reaction Chemistry & Engineering, 4(8): 1357-1386. https://doi.org/10.1039/C9RE00036D
- [69] Ye, L., Yang, W., Fan, J., Pu, X., Han, X., Qin, X., Ma, M., Huang, Z., Wang, T., Zhu, K., Xu, Y., Liu, J. (2024). The influence of pore-architecture over n-heptane cracking using MFI, \*BEA and MSE zeolite catalysts: Multipore versus hierarchical porosity. Chemical Engineering Journal, 482: 148705. https://doi.org/10.1016/j.cej.2024.148705
- [70] Javdani, A., Ahmadpour, J., Yaripour, F. (2019). Nanosized ZSM-5 zeolite synthesized via seeding technique for methanol conversions: A review. Microporous and Mesoporous Materials, 284: 443-458. https://doi.org/10.1016/j.micromeso.2019.04.063
- [71] Yi, F., Xu, D., Tao, Z., Hu, C., Bai, Y., Zhao, G., Chen, H., Cao, J.P., Yang, Y. (2022). Correlation of Brønsted acid sites and Al distribution in ZSM-5 zeolites and their effects on butenes conversion. Fuel, 320: 123729. https://doi.org/10.1016/j.fuel.2022.123729
- [72] Lo, B.T.W., Lin, W.C., Li, M.M.J., Day, S., Tang, C., Tsang, S.C.E. (2020). Evaluation of Brønsted and Lewis acid sites in H-ZSM-5 and H-USY with or without metal modification using probe molecule-synchrotron X-ray powder diffraction. Applied Catalysis A: General, 596:

- 117528. https://doi.org/10.1016/j.apcata.2020.117528
- [73] Woolery, G.L., Kuehl, G.H., Timken, H.C., Chester, A.W., Vartuli, J.C. (1997). On the nature of framework Brønsted and Lewis acid sites in ZSM-5. Zeolites, 19(4): 288-296. https://doi.org/10.1016/S0144-2449(97)00086-9
- [74] Gunawan, M., Novita, T., Aprialdi, F., Aulia, D., Nanda, A., Rasrendra, C., Addarojah, Z., Mujahidin, D., Kadja, G.T.M. (2023). Palm-oil transformation into green and clean biofuels: Recent advances in the zeolite-based catalytic technologies. Bioresource Technology Reports, 23: 101546. https://doi.org/10.1016/j.biteb.2023.101546
- [75] Engtrakul, C., Mukarakate, C., Starace, A.K., Magrini, K.A., Rogers, A.K., Yung, M.M. (2016). Effect of ZSM-5 acidity on aromatic product selectivity during upgrading of pine pyrolysis vapors. Catalysis Today, 269: 175-181. https://doi.org/10.1016/j.cattod.2015.10.032
- [76] Mancinelli, M., Precisvalle, N., Ardit, M., Beltrami, G., Gigli, L., Catizzone, E., Migliori, M., Giordano, G., Martucci, A. (2023). Thermal stability of templated ZSM-5 zeolites: An in-situ synchrotron X-ray powder diffraction study. Microporous and Mesoporous Materials, 362: 112777. https://doi.org/10.1016/j.micromeso.2023.112777
- [77] Hoff, T.C., Thilakaratne, R., Gardner, D.W., Brown, R.C., Tessonnier, J.P. (2016). Thermal stability of aluminum-rich ZSM-5 zeolites and consequences on aromatization reactions. The Journal of Physical Chemistry C, 120(36): 20103-20113. https://doi.org/10.1021/acs.jpcc.6b04671
- [78] Das, M., Dasgupta, S., Klunk, M.A., Xavier, S.J.S., Chemale Junior, F., Wander, P.R. (2020). Study involving removal of azo dye Direct Orange 34 by adsorption in zeolite-clay system. Canadian Journal of Chemistry, 98(8): 609-615. https://doi.org/10.1139/cjc-2020-0142
- [79] Fernandes, I.J., Calheiro, D., Kieling, A.G., Moraes, C.A.M., Rocha, T.L.A.C., Brehm, F.A., Modolo, R.C.E. (2016). Characterization of rice husk ash produced using different biomass combustion techniques for energy. Fuel, 165: 351-359. https://doi.org/10.1016/j.fuel.2015.10.086
- [80] Moraes, C.A.M., Fernandes, I.J., Calheiro, D., Berwanger Filho, J.A., Kieling, A.G., Rigon, M.R., Brehm, F.A., Schneider, I.A.H., Osório, E. (2014). Review of the rice production cycle: By-products and the

- main applications focusing on rice husk combustion and ash recycling. Waste Management & Research, 32(11): 1034-1048. https://doi.org/10.1177/0734242X14557379
- [81] Klunk, M.A., Das, M., Dasgupta, S., Caetano, N.R., Xavier, S.J.S., Souza, D.M., Wander, P.R., Moraes, C.A.M. (2021). Synthesis of ZSM-5 zeolite from metakaolin and rice husk ash to CO<sub>2</sub> adsorption. ECS Journal of Solid State Science and Technology, 10(1): 013001. https://doi.org/10.1149/2162-8777/abdb18
- [82] Kirdeciler, S.K., Akata, B. (2020). One pot fusion route for the synthesis of zeolite 4A using kaolin. Advanced Powder Technology, 31(10): 4336-4343. https://doi.org/10.1016/j.apt.2020.09.012
- [83] Chaikittisilp, W., Yokoi, T., Okubo, T. (2008). Crystallization behavior of zeolite beta with balanced incorporation of silicon and aluminum synthesized from alkali metal cation-free mixture. Microporous and Mesoporous Materials, 116(1-3): 188-195. https://doi.org/10.1016/j.micromeso.2008.04.001
- [84] Dasgupta, S., Klunk, M.A., Das, M., Xavier, S.J.S., Chemale, F., Wander, P.R., Moraes, C.A.M. (2021a). Hydrothermal synthesis of zeolite Y from green materials. Canadian Journal of Chemical Engineering, 99(S1): S179-S189. https://doi.org/10.1002/cjce.23994
- [85] Esmaeili, N., Boyd, S.E., Brown, C.L., Gray, E.M.A., Webb, C.J. (2019). Improving the gas-separation properties of PVAc-zeolite 4A mixed-matrix membranes through nano-sizing and silanation of the zeolite. ChemPhysChem, 20(12): 1590-1606. https://doi.org/10.1002/cphc.201900423
- [86] Nakrani, D., Belani, M., Bajaj, H.C., Somani, R.S., Singh, P.S. (2017). Concentrated colloidal solution system for preparation of uniform Zeolite-Y nanocrystals and their gas adsorption properties. Microporous and Mesoporous Materials, 241: 274-284. https://doi.org/10.1016/j.micromeso.2016.12.039
- [87] Lei, W., Li, L., Chen, X. (2022). Fast synthesis of hierarchical nanosized pure Si-Beta zeolite with low organic template content via the solvent-free method. Journal of Solid State Chemistry, 308: 122899. https://doi.org/10.1016/j.jssc.2022.122899
- [88] Xing, M., Zhang, L., Cao, J., Han, Y., Wang, F., Hao, K., Huang, L., Tao, Z., Wen, X., Yang, Y., Li, Y. (2022). Impact of the aluminum species state on Al pairs formation in the ZSM-5 framework. Microporous and Mesoporous Materials, 334: 111769. https://doi.org/10.1016/j.micromeso.2022.111769